Numerical Harmonic Analysis on the Hyperbolic Plane

Buma Fridman, Peter Kuchment, Kirk Lancaster,
Serguei Lissianoi, Mila Mogilevsky, Daowei Ma,
Igor Ponomarev, and Vassilis Papanicolaou
Mathematics and Statistics Department
Wichita State University
Wichita, KS 67260-0033, U.S.A.

Abstract

Results are reported of a numerical implementation of the hyperbolic Fourier transform and the geodesic and horocyclic Radon transforms on the hyperbolic plane, and of their inverses. The study is motivated by the hyperbolic geometry approach to the linearized inverse conductivity problem, suggested by C. A. Berenstein and E. Casadio Tarabusi.

1 Introduction

This paper was motivated by an approach to the inverse conductivity problem, which can be formulated as follows. Let $U \subset \mathbf{R}^n$ be a domain with boundary Γ. An unknown function σ (the conductivity) must be recovered from the following data. Given a function ψ on Γ (the current), one solves the Neumann boundary value problem

$$\begin{cases} \nabla \cdot (\sigma \nabla u) = 0 \quad in \quad U \\ \sigma \frac{\partial u}{\partial \nu}\big|_\Gamma = \psi, \end{cases}$$

where ν is the unit outer normal vector on Γ. Then one measures the boundary value $\phi = u|_\Gamma$ (the potential). All pairs (ψ, ϕ) are assumed to be accessible. In other words, the so-called Dirichlet-to-Neumann operator $\Lambda_\sigma : \phi \to \psi$ is known. One needs to recover the conductivity σ from this data. The problem, which amounts to inverting the mapping $\sigma \to \Lambda_\sigma$, is obviously nonlinear.

The practical version of this problem is the so-called Electrical Impedance Tomography, or Electrical Impedance Imaging. It has many important applications in medical diagnostics, engineering, and other areas. One can find detailed discussion of the inverse

conductivity problem and of the impedance tomography in [1]-[3], [14], [18]-[20], [22], and [26]-[32].

The inverse conductivity problem is very challenging analytically and numerically. There are several important problems to resolve: uniqueness of determination of the conductivity, stability of the reconstruction, and good inversion algorithms. While the problem of uniqueness can be considered as essentially solved (see [24], [31], [32], and references therein), the other problems are still far from a complete resolution. The problem is highly unstable, so there is probably no hope to achieve the quality of reconstruction known to other common tomographic techniques.

The first practical algorithm of D. Barber and B. Brown deals with the linearized problem (which is still very unstable). A thorough investigation of this algorithm was started by F. Santosa and M. Vogelius in [28]. The study done in [28] was extended by C. Berenstein and E. Casadio Tarabusi [8], [9] to an understanding that the linearized two-dimensional problem can be treated by means of hyperbolic integral geometry. Let us briefly explain how hyperbolic geometry can arise here. Consider the two-dimensional case when the domain U is the unit disc D in $\mathbb{C}$. It is well known (see [4] and [15]) that the unit disc serves as a model of the hyperbolic plane $\mathbb{H}^2$. We will pinpoint now the indications that hyperbolic geometry might play some role in the inverse conductivity problem (at least in its linearized formulation). First of all, the Laplace operator that arises in the linearized problem (see below) is invariant with respect to the group of Möbius transformations. Another indication is that if one creates a dipole current through a point on the boundary of D, then the equipotential lines and the current lines form families of geodesics and horocycles in $\mathbb{H}^2$. Following the analysis done in [28] of the algorithm suggested in [1], [2], C. Berenstein and E. Casadio Tarabusi discovered that in fact for $n = 2$ the linearized inverse conductivity problem can be reduced to the following integral geometry problem on $\mathbb{H}^2$: the measured data enables one to find the function

$$R_G(A * \sigma),$$

where R_G is the geodesic Radon transform on $\mathbb{H}^2$, A is an explicitly described radial function on $\mathbb{H}^2$, and the star $*$ denotes the (non-Euclidean) convolution on $\mathbb{H}^2$. Now known tools of harmonic analysis on $\mathbb{H}^2$ (including inversion of the geodesic Radon transform, an analog of Fourier transform, and convolution operators) enable one to recover σ. One can find descriptions and properties of these transforms in [15]. A generalization of this approach to dimensions greater than two was obtained in [13], where it was shown that the higher dimensional case requires a combination of methods of Euclidean and hyperbolic integral geometries.

If one wants to use this approach to the inverse conductivity problem numerically, the problem arises of numerical implementation of harmonic analysis on the hyperbolic plane. Namely, one needs to be able to compute the following transforms and their inverses: Fourier transform, geodesic Radon transform, and horocyclic Radon transform on the hyperbolic plane. Implementation of these transforms was the goal of the work, the

results of which are described in this paper. Most of the work was done during sessions of a tomography seminar at WSU, which explains the large number of authors involved. This report was presented during the 1st ISAAC Congress in Delaware in 1977, but by a mistake was omitted from its Proceedings.

2 A review of harmonic analysis on the hyperbolic plane

Details of harmonic analysis on $\mathbb{H}^2$ and of its application to the inverse conductivity problem can be found in [15]-[17], [5]-[9], [13], and [23]. We will only briefly remind the reader some basics of analysis on $\mathbb{H}^2$ (see [15]).

The unit disk D in $\mathbb{C}$ with the metric

$$ds^2 = \frac{|dz|^2}{(1-|z|^2)^2}$$

is a model of $\mathbb{H}^2$ (the Poincare model). The **group of Möbius transformations** consists of the isometries

$$z \to \frac{az+b}{\overline{b}z+\overline{a}},\ |a|^2-|b|^2=1.$$

The **invariant Laplacian** is

$$\Delta_H = (1-|z|^2)^2\Delta = 4(1-|z|^2)^2\frac{\partial^2}{\partial z\partial\overline{z}}.$$

The geodesics are arcs of circles orthogonal to the boundary ∂D. The **geodesic Radon transform** of a function f on D is defined as follows:

$$(R_G f)(\gamma) = \int\limits_{\gamma} f(z)ds,$$

where γ is a geodesic. The dual transform (which in analogy with tomography can be called the **geodesic backprojection**) is defined as follows:

$$(R_G^{\#} g)(z) = \int\limits_{\gamma\in\Gamma_z} g(\gamma)d\mu_z(\gamma),$$

where Γ_z is the set of all geodesics passing through the point z, and μ_z is the normalized measure on Γ_z invariant with respect to the isotropy subgroup of the point z.

Horocycles are the circles in D tangent to the boundary ∂D. The **horocyclic Radon transform** of a function $f(z)$ on D is

$$(R_H f)(\zeta) = \int\limits_{\zeta} f(z)ds,$$

where ζ is a horocycle. A **horocyclic backprojection** operator can be defined analogously to the geodesic one.

In order to describe the Fourier transform on $\mathbb{H}^2$ (see[15]), we recall first how the Fourier transform is defined in the Euclidean case. A function $f(x)$ is integrated being multiplied first by functions $e_{\lambda,\omega}(x)$:

$$f \to \widetilde{f}(\lambda) = \int f(x)e_{\lambda,\omega}(x)dx.$$

Here $e_{\lambda,\omega}(x)$ is the exponent

$$e_{\lambda,\omega}(x) = e^{i\lambda\langle x,\omega\rangle},$$

where ω is a unit vector in $\mathbb{R}^n$, $\lambda \in \mathbb{C}$, and $\langle x, \omega\rangle$ denotes the standard scalar product (which can also be understood as the signed distance from 0 to the plane through the point x orthogonal to ω). The characteristic properties of these exponentials are that they are plane waves (i.e., $e_{\lambda,\omega}$ is constant on planes orthogonal to ω) and they are joint eigenfunctions of all constant coefficient linear differential operators in $\mathbb{R}^n$:

$$Le_{\lambda,\omega} = L(\lambda)e_{\lambda,\omega},$$

where $L = L(\mathcal{D})$, and $\mathcal{D} = \frac{1}{i}\frac{\partial}{\partial x}$.

This definition of the Fourier transform can be generalized to the case of the hyperbolic plane (see [15]). Let us denote by $\langle z, b\rangle$ the signed (hyperbolic) distance from 0 to the horocycle through points $b \in \partial D$ and $z \in D$. Then the "plane waves"

$$e_{\lambda,b}(z) = e^{(-i\lambda+1)\langle z,b\rangle},\ \lambda \in \mathbb{R},\ b \in B = \partial D$$

are natural analogs of exponents in the Euclidean case. These functions are related to the Poisson's kernel

$$P(z,b) = \frac{1-|z|^2}{|z-b|^2}, z \in D, b \in B = \partial D$$

as follows:

$$e^{2\langle z,b\rangle} = P(z,b).$$

Additional similarity with the Euclidean case can be seen in the fact that these functions are joint eigenfunctions of all invariant linear differential operators on $\mathbb{H}^2$ (see [15]). Now one can define the **hyperbolic Fourier transform** as follows:

$$f(z) \to \widetilde{f}(\lambda, b) = \int f(z)e_{\lambda,b}(z)d\mu(z).$$

There is a relation

$$\widetilde{f} = \mathcal{F} R_H f, \tag{1}$$

with the horocyclic Radon transform R_H, where $\mathcal{F}$ is the 1-dimensional Euclidean Fourier transform. This relation is analogous to the so called Fourier slice (or projection slice) theorem in tomography [25]. Properties of this Fourier transform are described in [15].

3 Inversion of Fourier and Radon transforms on the hyperbolic plane

A Fourier inversion formula was obtained by Helgason [15]:

$$f(z) = \frac{1}{4\pi} \int_{\mathbb{R}} \int_{\partial D} \widetilde{f}(\lambda, b) e^{(i\lambda+1)\langle z,b\rangle} \lambda \, th \frac{\pi\lambda}{2} d\lambda db. \tag{2}$$

Together with formula (1), this also provides a method of inverting the horocyclic Radon transform R_H.

Inversion of the geodesic Radon transform was provided in different forms by S. Helgason [16] and by C. A. Berenstein and E. Casadio Tarabusi [5].

Helgason's formula is an analog of Radon's original formula:

$$f = \frac{2}{\pi} \left[\left(\frac{d}{d(u^2)} \right) \int_0^u \left(R^{\#}_{cosh^{-1}(1/v)} (R_G f) \right) \left(u^2 - v^2 \right)^{-1/2} dv \right]_{v=1}, \tag{3}$$

where $R^{\#}_p$ is the backprojection-type operator that integrates over the set of geodesics passing at a distance p from a given point.

The formula provided by Berenstein and Casadio Tarabusi is

$$4\pi f = -\Delta S R^{\#}_G R_G f,$$

where Δ is the Laplace-Beltrami operator and S is the operator of convolution with an explicitly given radial kernel. This is an analog of the so called ρ-filtered backprojection algorithm in tomography.

A formula that happened to be more convenient for our purpose was obtained by S. Lissianoi and I. Ponomarev [23]. This formula can be derived from (3). It is an analog of the filtered backprojection formula in tomography, which enables one to use the standard one-dimensional FFT for inversion:

$$f(z) = \\ -\frac{(1-|z|^2)^2}{4\pi^2} \int_{S^1} \frac{1}{|s-z|^4} \left(\int_{-\infty}^{\infty} \left(\frac{d}{dt} Rf \right) \left(t - \frac{Im\,(\overline{z}s)}{|s-z|^2}, s \right) \frac{dt}{t} \right) |ds|\,. \tag{4}$$

Here the following parametrization of geodesics is used:

$$\xi = \{x, s\} = \{z \in D \mid Im(z\overline{s} - 1)^{-1} = x, x \in \mathbb{R}, s \in S^1 \subset \mathbb{C}\}.$$

4 Numerical implementation and results

Our goal was to implement numerically the hyperbolic Fourier transform, Radon transforms R_H and R_G, their duals $R_H^\#$ and $R_G^\#$, and their inverse operators. In the Euclidean case, the standard techniques involve usage of Shannon's sampling theorem and the FFT. Sampling is the first problem one encounters when trying to implement these transforms. Namely, one would want to have a tiling of the hyperbolic plane with "pixels" such that their (hyperbolic) sizes stay approximately constant, such that one can easily compute the lengths of intersections of these pixels with geodesics and horocycles, and such that it is possible to refine the mesh when needed. In the Euclidean case all these problems are easily resolved by choosing as pixels the fundamental domain of a lattice (a discrete subgroup of $\mathbb{R}^n$) and its translations with respect to this lattice. An additional advantage of such a choice is existence of the Fast Fourier Transform algorithm. However, the natural generalization of this approach to the hyperbolic case fails. Namely, if one wants to use a discrete subgroup of the Möbius group and sample functions at the points of an orbit of such a group, then such a mesh cannot be refined. The known rigidity theorems (see, for instance, Theorem 10.4.5 in [4]) show that there is a lower bound on the area of the fundamental domain for any such discrete subgroup. This means that pixels chosen as fundamental domains of discrete groups cannot be made arbitrarily small. After trying several different approaches (including usage of harmonic analysis on trees, rewriting the problem on a two-sheeted hyperboloid in $\mathbb{R}^3$, and some others), we decided to use the following one. First of all, a finite index subgroup G in a triangular group (see [4]) was chosen. The group G is a discrete group of Möbius transformations of the hyperbolic plane. Its fundamental domain is a heptagon S in $\mathbb{H}^2$. However, one cannot use this heptagon as a pixel, since it has a rather large size. On the other hand, the hyperbolic metric in this heptagon is rather close to the Euclidean one. Hence, it is a reasonable idea to use a rectangular Euclidean mesh inside of the heptagon, and then reproduce it in the translated copies of the fundamental domain by the corresponding Möbius transforms. This procedure is illustrated on Figure 1. In this figure the Euclidean mesh inside of the heptagon S extends to its neighborhood, and hence it overlaps with the mesh in the neighboring heptagons. In practical calculations these overlappings are eliminated. With this mesh we achieve our main goals: the hyperbolic sizes of pixels are approximately equal and lengths of intersections of geodesics and horocycles with the pixels can be easily computed by a computer code. One can successfully use here the capabilities of the C++ language, creating objects like fundamental domains, Möbius transforms, geodesics, and horocycles, and necessary operations on them.

After the sampling problem is resolved, one can numerically implement the Fourier and Radon operators and their inverses.

Geodesic and horocyclic Radon transforms are implemented in a standard way: given a function constant on pixels and a circular arc (a geodesic or a horocycle), one can compute the hyperbolic lengths of the intersections of the arc with all pixels in the support of the

function, and then discretize the integral. Now the Fourier transform on $\mathbb{H}^2$, according to formula (1), can be computed as the composition of the horocyclic Radon transform with the standard 1-dimensional FFT.

Inversion of the Fourier transform, according to formula (2), can be done by composition of the following operations: multiplication by the weight function $\lambda\, th\,(\pi\lambda/2)$, 1-dimensional FFT, multiplication by $e^{\langle z,b\rangle}$, and averaging over ∂D. (The latter one is the standard backprojection in tomography [25].)

Formula (1) says that by inverting the Fourier transform on $\mathbb{H}^2$, one can simultaneously invert the horocyclic Radon transform. Namely, knowing the horocyclic Radon image of a function, one performs a 1-dimensional FFT, and then inverts the hyperbolic Fourier transform.

Inversion of the geodesic Radon transform can be implemented according to formula (4). This formula can be rewritten as

$$f(z) = \frac{(1-|z|^2)^2}{4\pi^2}\left(R^{\#}\left[\frac{H\frac{d}{dt}\left(R_G f\right)(t,s)}{|s-z|^2}\right]\right)(z).$$

Here H is the Hilbert transform, and $R^{\#}$ is an averaging operator over a circle (a backprojection). Hence, the inversion procedure involves multiplication by a weight function, 1-dimensional FFT, filtration in the Fourier domain (in order to account for the differentiation and Hilbert transform), inverse FFT, and a backprojection (averaging over a circle).

Figures 2 through 5 (according to the Fourier-slice formula (1)) simultaneously represent inversions of both the horocyclic Radon transform and the Fourier transform.

Figure 2 shows the reconstruction of the characteristic function of the central heptagon.

Figures 3 and 4 represent reconstructions of characteristic functions of chess-board phantoms located in different copies of the fundamental domain S.

Figure 5 shows the local tomographic reconstruction of the singularities of a chess-board phantom (see [21] for the description of the procedure and [10]-[12] for a general discussion of local tomography).

Figure 6 contains the reconstruction of a chessboard phantom intersected with the central heptagon from its geodesic Radon transform.

Finally, Figure 7 represents a reconstruction from the geodesic Radon data of a phantom consisting of the central heptagon S overlapped with a part of a disk.

The significance of this kind of example is that since the phantom intersects several copies of the fundamental domain, and since the mesh undergoes changes across the boundaries of these domains, one can expect artifacts along these boundaries. The reconstruction,

however, behaves well along the boundary. All reconstructions were done with a rather small number of projections, which explains some artifacts. Namely, 64 projections were chosen for both horocyclic and geodesic Radon transforms, and 64 horocycles or geodesics in each projection.

5 Acknowledgment

The authors thank Professor P. Parker for helpful comments. This work was supported in part by an NSF EPSCoR grant. The authors express their gratitude to the NSF and State of Kansas for this support.

References

[1] D.C. Barber, B.H. Brown, *Applied potential tomography*, J. Phys. E.: Sci. Instrum. 17(1984), 723-733.

[2] D.C. Barber, B.H. Brown, *Recent developments in applied potential tomography-APT*, in: Information Processing in Medical Imaging, Nijhoff, Amsterdam, 1986, 106-121.

[3] D.C. Barber, B.H. Brown, *Progress in electrical impedance tomography*, in "Inverse Problems in Partial Differential Equations", SIAM, 1990, p. 151-164.

[4] A. Berdon, *The Geometry of Discrete Groups*, Springer Verlag, New York-Heidelberg-Berlin, 1983.

[5] C. Berenstein, E. Casadio Tarabusi, *Inversion formulas for the k-dimensional Radon transform in real hyperbolic spaces*, Duke Math. J. 62(1991),no.3, 613- 631.

[6] C. Berenstein, E. Casadio Tarabusi, *On the Radon and Riesz transforms in real hyperbolic spaces*, Contemp. Math. 140(1992), 1-21.

[7] C. Berenstein, E. Casadio Tarabusi, *Range of the k-dimensional Radon transform in real hyperbolic spaces*, Forum. Math. 5(1993), 603-616.

[8] C. Berenstein, E. Casadio Tarabusi, *The inverse conductivity problem and the hyperbolic X-ray transform*, in: "75 years of Radon transform (Vienna 1992)", 39-44, Internat. Press, Cambridge, MA 1994.

[9] C. Berenstein, E. Casadio Tarabusi, *Integral geometry in hyperbolic spaces and electrical impedance tomography*, SIAM J. Appl. Math. 56(1996), no.3, 755-764.

[10] A. Faridani, F. Keinert, F. Natterer, E. L. Ritman, and K. T. Smith, *Local and global tomography*, in Signal Processing, Part II, 241–255, IMA Vol. Math. Appl., 23, Springer, New York, 1990.

[11] A. Faridani, E.L. Ritman, and K.T. Smith, *Local tomography*, SIAM J. Appl. Math. 52 (1992), no. 2, 459–484.

[12] A. Faridani, E.L. Ritman, and K.T. Smith, *Examples of local tomography*, SIAM J. Appl. Math. 52 (1992), no. 4, 1193–1198.

[13] B. Fridman, P. Kuchment, D. Ma, and V. Papanicolaou, *Solution of the linearized inverse conductivity problem in the half space via integral geometry*, p. 85-95, in "Voronezh Winter Mathematical Schools", AMS, Providence, RI, 1998

[14] A. Friedman, M. Vogelius, *Determining cracks by boundary measurements*, Ind. Univ. Math. J. 38(1989), 527-556.

[15] S. Helgason, *Groups and Geometric Analysis: Integral Geometry, Invariant Differential Operators, and Spherical Functions*, Pure and Appl. Math., vol. 113, Academic Press, Orlando, FL, 1984.

[16] S. Helgason, *The totally-geodesic Radon transform on constant curvature spaces*, Contemp. Math. 113(1990), 141-149.

[17] S. Helgason, *Geometric Analysis on Symmetric Spaces*, AMS, Providence, RI 1994.

[18] D. Isaacson and M. Cheney, *Current problems in impedance imaging, in* "Inverse Problems in Partial Differential Equations", SIAM, 1990, p. 141-149.

[19] V. Isakov, *Inverse Problems for Partial Differential Equations*, New York: Springer-Verlag, 1998.

[20] R. Kohn, M. Vogelius, *Determining conductivity by boundary measurements, I*, Comm. Pure Appl. Math., 37(1984), 289-298; II, 38(1985), 643-667.

[21] P. Kuchment, K. Lancaster, and L. Mogilevskaya, *On the local tomography*, Inverse Problems, 11(1995), 571-589.

[22] V. Liepa, F. Santosa, and M. Vogelius, *Crack determination from boundary measurements - reconstruction from experimental data*, J. Nondestructive Evaluation 12(1993), 163-173.

[23] S. Lissianoi and I. Ponomarev, *On the inversion of the geodesic Radon transform on the hyperbolic plane*, Inverse Problems 13(1997), no. 4, 1053–1062.

[24] A. Nachman, *Global uniqueness for a two-dimensional inverse boundary value problem*, Ann. Math. 143(1996), no.1, 71-96.

[25] F. Natterer, *The Mathematics of Computerized Tomography*, Teubner, Stuttgart, 1986.

[26] E.T. Quinto, M. Cheney, and P. Kuchment (Editors), *Tomography, Impedance Imaging, and Integral Geometry*, Lectures in Appl. Math., vol. 30, AMS, Providence, RI 1994.

[27] F. Santosa, *Inverse problem holds key to safe, continuous imaging*, SIAM News, 27(1994), no.6.

[28] F. Santosa, M. Vogelius, *A backprojection algorithm for electrical impedance imaging*, SIAM J. Appl. Math., 50 (1990), 216-241.

[29] E. Somersalo, M. Cheney, D. Isaacson, E. Isaacson, *Layer-stripping : a direct numerical method for impedance imaging*, Inverse Problems, 7 (1991), 899- 926.

[30] J. Sylvester, *A Convergent layer-stripping algorithm for the radially symmetric impedance tomography problem*, Comm. in Part. Diff. Equat., 17 (1992), 1955-1994.

[31] J. Sylvester and G. Uhlmann, *The Dirichlet to Neumann map and its applications*, in "Inverse Problems in Partial Differential Equations", SIAM, 1990, p. 101-139.

[32] G. Uhlmann, *Inverse boundary value problems and applications*, Asterisque 207(1992), p. 153-211

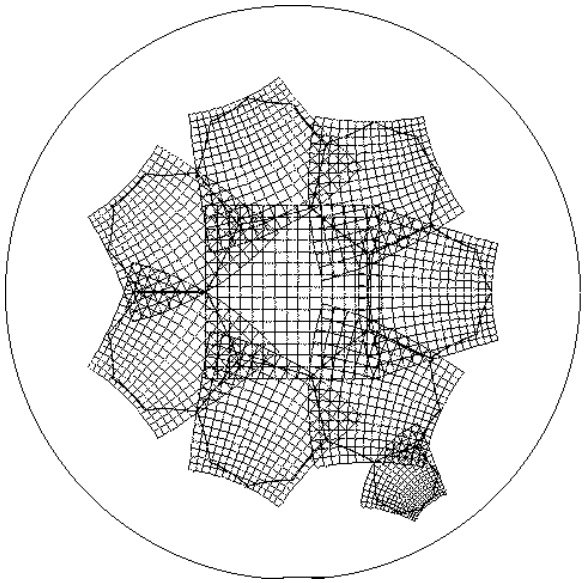

Figure 1:

Figure 2:

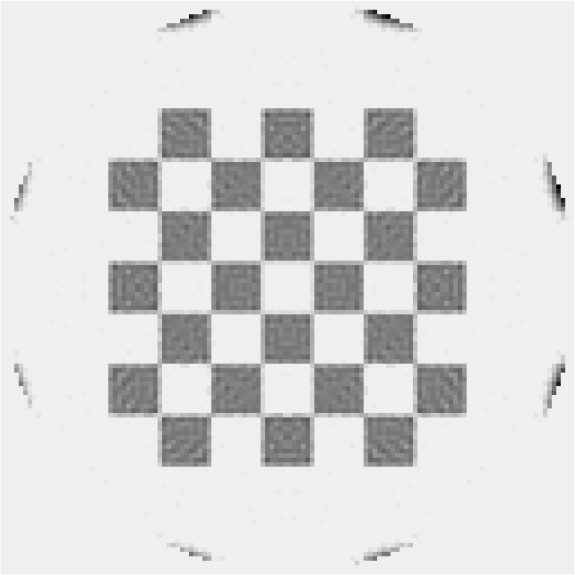

Figure 3:

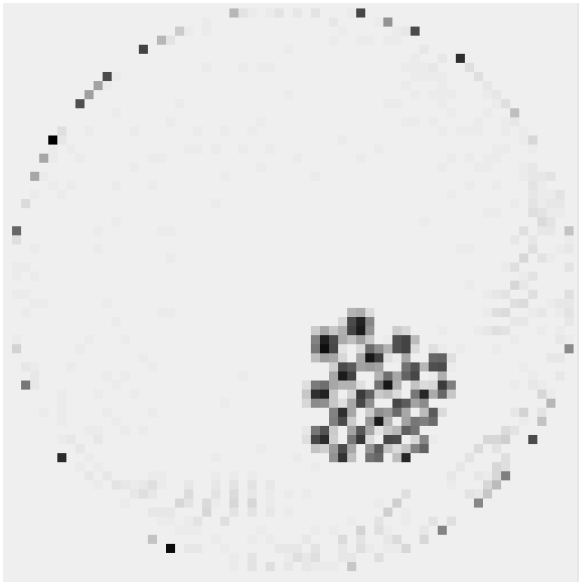

Figure 4:

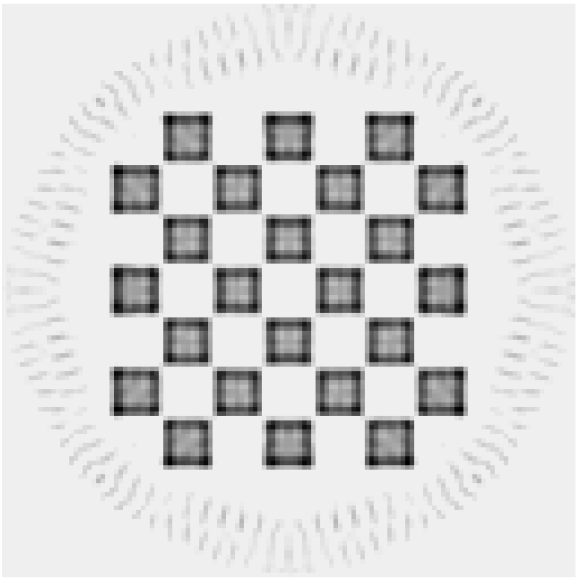

Figure 5:

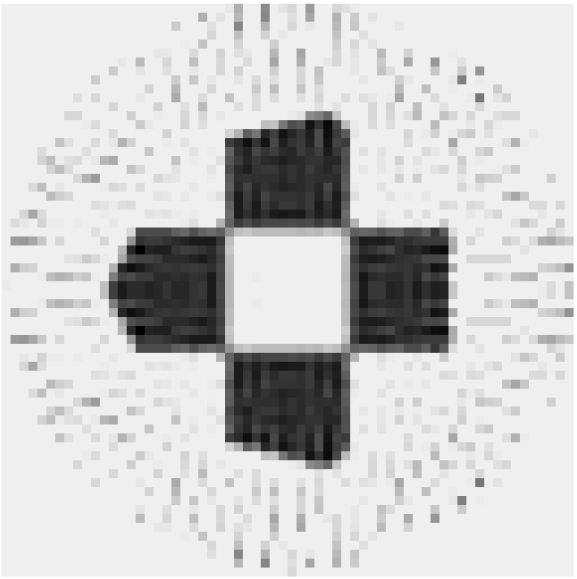

Figure 6:

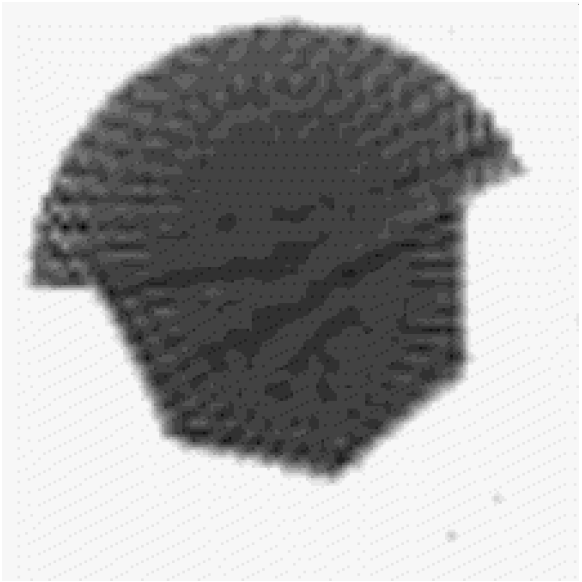

Figure 7: